

# Design and Optimization of Backfolded Piezoelectric Microenergy Generators

Master's thesis in Applied Mechanics

Viktor Sjöström

---

DEPARTMENT OF MECHANICS AND MARITIME SCIENCE

CHALMERS UNIVERSITY OF TECHNOLOGY

Gothenburg, Sweden 2021

[www.chalmers.se](http://www.chalmers.se)



MASTER'S THESIS 2021:24

Design and Optimization of Backfolded Piezoelectric Microenergy Generators

Viktor Sjöström



**CHALMERS**  
UNIVERSITY OF TECHNOLOGY

Department of Mechanics and Maritime Science  
*Division of Dynamics*  
CHALMERS UNIVERSITY OF TECHNOLOGY  
Gothenburg, Sweden 2021

Design and Optimization of Backfolded Piezoelectric Microenergy Generators  
Viktor Sjöström

© Viktor Sjöström, 2021.

Master's Thesis 2021:24  
Department of Mechanics and Maritime Science  
Division of Dynamics  
Chalmers University of Technology  
SE-412 96 Gothenburg  
Telephone +46 31 772 1000

Cover: Electric potential distribution on the surface of the double fold generator.

Chalmers Reproservice  
Gothenburg, Sweden 2021

Design and Optimization of Backfolded Piezoelectric Microenergy Generators  
Viktor Sjöström  
Department of Mechanics and Maritime Science  
Division of Dynamics  
Chalmers University of Technology

## Abstract

A piezoelectric micro generator is a device that is intended to supply power to a wireless internet of things (IoT) application. The generator accumulates power when undergoing mechanical stress by vibration from the surroundings. The micro generator is able to sustain power to the application without any external source of power.

The objective is to propose a design for two different models that is optimized with respect to bandwidth, tolerance and low frequency spectrum. The first model is a single back folded beam structure, while the second is a double folded beam structure. The optimisation was carried out with respect to resonant frequency analysis and frequency response of the design. The simulations were carried out with the finite element software COMSOL multiphysics 5.6 and post processed in Matlab. The total length, width of each beam and the length of the outer proof mass were the major factors in improvement of the bandwidth, tolerance and frequency spectrum. The final design of the single fold generator resulted in a bandwidth of 1181 Hz operating between 1100 and 2500 Hz with a tolerance of 236 %. The final design of the double fold generator resulted in a bandwidth of at least 2500 Hz operating between 900 and 2500 Hz with a tolerance of 27.6 % and 50.1 %. The bandwidth for both models were calculated with respect to a 0.1 V threshold.

Keywords: Energy generator, Piezoelectric, Bandwidth



## Acknowledgements

I would like to thank my supervisor Associate Professor Peter Folkow for the support throughout this project work. Peter has contributed with discussion and advice on how to advance with this project work. Additionally, I want to thank Lic. of Engineering Agin Vyas for explaining limitations and fabrication process of piezoelectric micro generators. I would also like to thank Johan Andersson for his previous work on piezoelectric micro energy harvester. His work has been the foundation for this project work.

Viktor Sjöström, Gothenburg, June 2021



# Contents

<b>List of Figures</b>	<b>ix</b>
<b>List of Tables</b>	<b>x</b>
<b>1 Introduction</b>	<b>1</b>
1.1 Background . . . . .	1
1.2 Limitations . . . . .	2
1.3 Aim . . . . .	2
<b>2 Methodology</b>	<b>3</b>
2.1 Geometry . . . . .	3
2.1.1 Single Fold Generator . . . . .	3
2.1.2 Double Fold Generator . . . . .	4
2.2 FE-Analysis . . . . .	5
2.2.1 Piezoelectric model . . . . .	5
2.2.1.1 Boundary Condition . . . . .	6
2.2.1.2 Damping . . . . .	6
2.2.2 Simulation Approach . . . . .	7
2.2.2.1 Analysis of Eigenfrequency and Modes Shape . . . . .	7
2.2.2.2 Analysis of frequency response . . . . .	7
2.2.3 Post processing . . . . .	7
<b>3 Results</b>	<b>9</b>
3.1 Single Fold Generator . . . . .	9
3.1.1 Eigenfrequencies and mode shape . . . . .	9
3.1.2 Frequency Response . . . . .	12
3.2 Double Fold Generator . . . . .	16
3.2.1 Eigenfrequencies and mode shape . . . . .	16
3.2.2 Frequency Response . . . . .	19
<b>4 Discussion</b>	<b>23</b>
<b>5 Conclusion</b>	<b>25</b>
<b>Bibliography</b>	<b>26</b>
<b>A Appendix</b>	<b>I</b>
A.1 Final Design, Single Fold Generator . . . . .	I
A.2 Final Design, Double Fold Generator . . . . .	II

# List of Figures

2.1	Schematic view from above of the single fold generator. . . . .	3
2.2	Schematic view from the side of the single fold generator. . . . .	4
2.3	Schematic overview of the double fold generator. . . . .	4
2.4	Schematic side view of the double fold generator. . . . .	5
2.5	Initial geometry in COMSOL of the Single fold (a) and the double fold generator (b). . . . .	6
2.6	Illustration of bandwidth and tolerance on the frequency response curve. . . . .	8
3.1	Frequency study with a parameter sweep over different outer beam lengths. . . . .	9
3.2	Second mode shape of the single fold generator showing in plane motion. The deflection is not to scale. . . . .	10
3.3	Frequency study with a parameter sweep over different outer beam widths. . . . .	10
3.4	First mode shape of the single fold generator. The deflection is not to scale. . . . .	11
3.5	Second mode shape of the single fold generator. The deflection is not to scale. . . . .	11
3.6	Frequency response for three different measures of the outer proof mass $l_{po}$ . . . . .	12
3.7	Frequency response of three different measures of the inner proof mass $l_{pi}$ . . . . .	13
3.8	Bandwidth for three different measures of the inner proof mass length $l_{pi}$ . . . . .	13
3.9	Frequency response for each PZT covered beam. . . . .	14
3.10	Frequency response of the total output from the structure. . . . .	14
3.11	Mesh convergance plot for with respect to bandwidth $b_f$ (upper) and tolerance $\delta$ (lower). . . . .	15
3.12	Frequency study with a parameter sweep over different outer beam lengths . . . . .	16
3.13	Second mode shape of the double fold generator showing in plane motion. . . . .	16
3.14	Frequency study with a parameter sweep over different outer beam widths. . . . .	17
3.15	Frequency study with a parameter sweep over different outer beam widths. . . . .	18
3.16	updated geometry of the double fold generator showing first mode shape (a), second mode shape (b) and the third mode shape(c). The movement is not to scale. . . . .	18
3.17	Frequency response of three different measures of the outer proof mass $l_{po}$ . . . . .	19
3.18	Frequency response of three different measures of the inner proof mass $l_{pi}$ . . . . .	20
3.19	Frequency response of three different measures of the inner proof mass $l_{pi}$ . . . . .	21
3.20	Frequency response of the total output from the structure . . . . .	21
3.21	Mesh convergance plot for with respect to the first tolerance $\delta_1$ (upper) and second tolerance $\delta_2$ (lower). . . . .	22

# List of Tables

2.1	Initial design parameters for the single fold generator. All measures are in $\mu\text{m}$ . . .	4
2.2	Initial design parameters for the double fold generator. All measures are in $\mu\text{m}$ . . .	5
3.1	Final design parameters for the single fold generator. All measures are in $\mu\text{m}$ . . .	15
3.2	Final design parameters for the double fold generator. All measures are in $\mu\text{m}$ . . .	22

# 1

## Introduction

Microsystems are becoming increasingly smaller and integrated. With this, the demand for power and smart solutions are also increasing. The vision is to have an entirely Internet of Things (IoT) based platform that can operate by itself with a wireless source of power. This source can be in the form of a vibration-based energy generator with an energy storage unit. The energy generator is a suitable candidate for an on-chip harvesting system that is subjected to vibration in the surroundings. However, a disadvantage of these energy generators is their narrow bandwidth of harvestable frequencies [1]. Difficulties arise when scaling down the energy generator as the bandwidth broadening solution cannot easily be scaled down. Furthermore, the manufacturing process is complicated and expensive. This means that the energy harvester needs to be optimised in order to be a competitive power solution. This thesis work is a further development from a previous study on back folded energy harvester done by Andersson [2]. His study was carried out with a material layout of silicon and lead zirconate titanate (PZT) with a thickness of 20  $\mu\text{m}$  and 1  $\mu\text{m}$  respectively. However, a PZT thickness less than 2  $\mu\text{m}$  usually results in low voltage and power output. This may be improved by increasing the thickness of the PZT layer on the generator [3].

### 1.1 Background

A piezoelectric microenergy generator is a device that is partly made of a piezoelectric material. This material accumulates electricity when undergoing mechanical stress. This phenomenon is related to the crystalline structure of the material. A material that is commonly used in piezoelectric generator is PZT. This material has good piezoelectric properties and shaping flexibility. The ductile behavior leads to good workability of the material [4].

The energy generator gives maximum output by operating at the resonance frequency of the beam structure. This means that the design of the energy generator must be optimized with respect to the specific application it is intended to supply with power. Since most resonance frequencies are narrow, the operating bandwidth is limited to a small range of frequencies. One example is to have several single cantilever beams in an array that is designed to operate at different resonance frequencies. By having the resonance frequencies overlapping each other, the total operating bandwidth may be widened. A negative aspect of this arrangement is that it requires relatively much space to operate and the fabrication process is complex [5].

Another way to achieve wide bandwidth is to have a design that has multiple resonance frequencies within the frequency range. If the resonance frequencies are close enough, the inter resonance peak will rise, thus widening the operating bandwidth [6]. This design may take the form of a back folded cantilever beam structure that utilizes multiple degrees of freedom. The back folded cantilever design consists of two outer beams that are connected with a proof mass. Between the outer beams, there is an inner beam connected to the proof mass, which may induce a second resonance frequency. This design is more space efficient and the planar design is advantageous regarding fabrication on micro scale [6]. Furthermore, the total electric potential output may be increased with a factor of 1.5 with the back folded design if compared with an array structure [7].

## 1.2 Limitations

Outer dimensions must be within the limit of one square centimeter. The boundary condition is simplified to a harmonic oscillation with constant amplitude. The simulations will be carried out with COMSOL Multiphysics 5.6 and post processed in Matlab. Geometric optimizing will be carried out with respect to manufacturing feasibility. A piezoelectric energy generator is usually fabricated with a wide range of different materials. A layup and fabrication process is explained in a study carried out by Vyas et al. In this study, the constituent in the structure starting from bottom was 20  $\mu\text{m}$  silicon, 500 nm silicon dioxide, 20 nm titanium, 100 nm platinum, 100 nm LaNiO, 1  $\mu\text{m}$  PZT, 20 nm titanium and at the top 100 nm platinum [8]. In this thesis work, the material layup is simplified to only include silicon and PZT.

## 1.3 Aim

The aim of this thesis is to propose a suitable design for two different energy generators with the purpose of supplying an IoT application with self sustaining power. The first design is a single back folded two degrees of freedom beam structure. The second design is an extension of the first design with an additional back folded beam structure. The designs will be optimized with an iteration process with respect to bandwidth, tolerance and low frequency spectrum where the bandwidth is operating.

# 2

## Methodology

### 2.1 Geometry

The geometry is divided into two different designs. The first model is the single fold generator, which is based on the final design proposed by Andersson [2]. This design was based on a layup of silicon and PZT with a thickness of 20 and 1  $\mu\text{m}$  respectively. The second design is the double fold generator, which is a further development of the single fold generator. In this study, both models used the same fixed thickness layup of a base layer of silicon with a thickness of 100  $\mu\text{m}$  and a PZT layer of 120  $\mu\text{m}$ . All proof masses on the single and double fold generator are defined to be the same thickness as the base silicon layer. This decision was made due to shortening the fabrication process of the generators.

#### 2.1.1 Single Fold Generator

The single fold generator consist of two outer beams which are connected with a outer proof mass. Between the outer beams, there is an inner beam with a proof mass attached to the end of the beam. A schematic view over the single fold generator is presented in Figure 2.1. The thickness and proof mass layup can be seen in Figure 2.2. The gray part represents the PZT layer in the structure, while the white part represents the silicon layer. The structure is symmetric over the dashed line. The outer beams are assumed to be fixed by a prescribed boundary condition. The initial parameter values can be seen in Table 2.1.

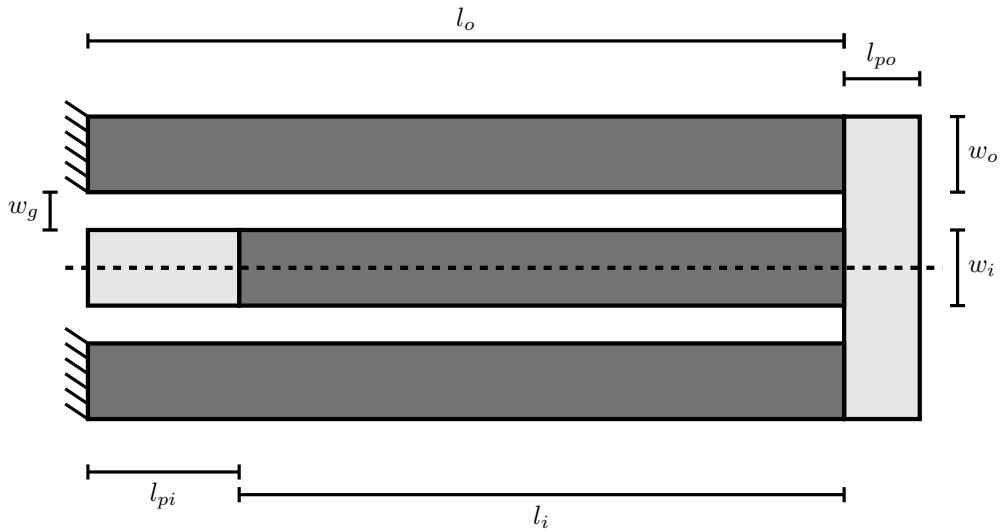


**Figure 2.1:** Schematic view from above of the single fold generator.



**Figure 2.2:** Schematic view from the side of the single fold generator.

**Table 2.1:** Initial design parameters for the single fold generator. All measures are in  $\mu\text{m}$

$l_o$	3000
$l_i$	2990
$l_{po}$	100
$l_{pi}$	0
$w_o$	200
$w_i$	400
$w_g$	50
$t_{po}$	0
$t_{pi}$	0
$t_{Si}$	100
$t_{PZT}$	120

### 2.1.2 Double Fold Generator

The double fold generator uses the same idea with two outer beams which are connected with a proof mass. The outer beams are also fixed by a prescribed boundary condition. The inner beam is split up with the addition of a single beam with added proof mass. A schematic overview of the beam can be seen in Figure 2.3. As previously mentioned, the side view in Figure 2.4 shows that the double fold generator uses the same material layup. This model uses the same initial dimensions as the single fold generator. The added middle beam is assumed to have the same initial width as the inner beams.

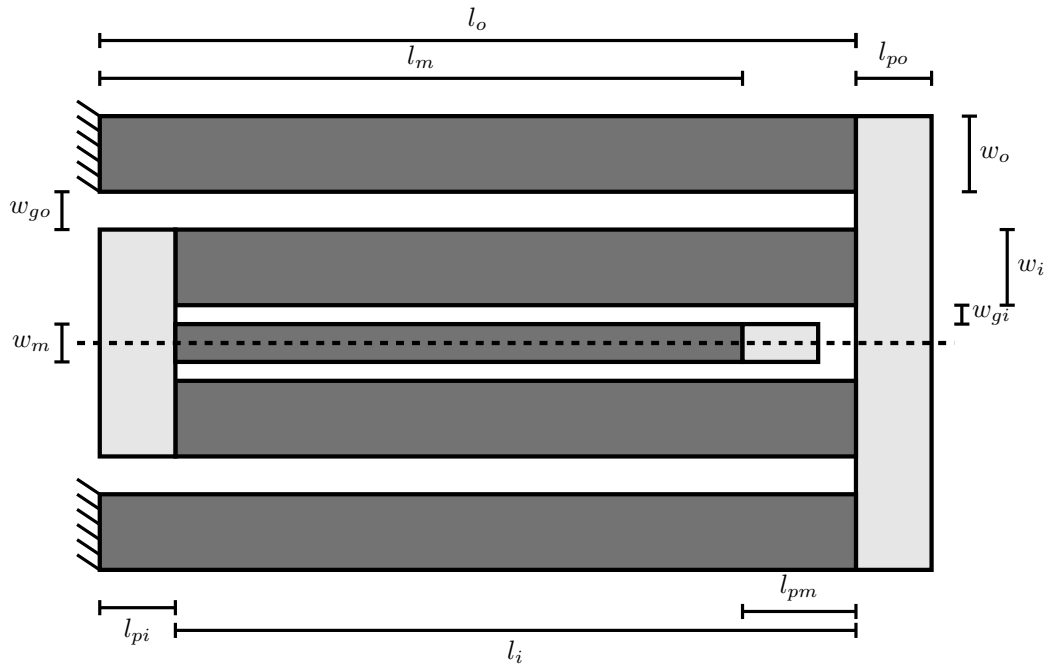


**Figure 2.3:** Schematic overview of the double fold generator.

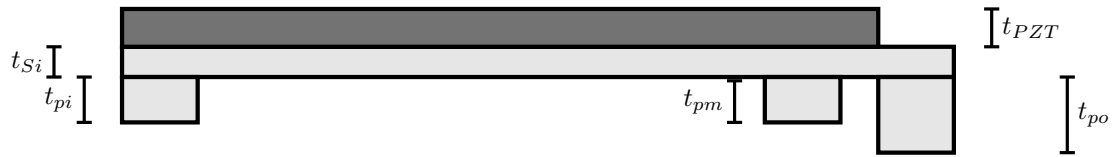


**Figure 2.4:** Schematic side view of the double fold generator.

**Table 2.2:** Initial design parameters for the double fold generator. All measures are in  $\mu\text{m}$ .

$l_o$	3000
$l_i$	2990
$l_m$	2980
$l_{po}$	100
$l_{pi}$	0
$l_{pm}$	0
$w_o$	200
$w_i$	400
$w_{go}$	50
$w_{gi}$	$w_{go}$
$w_m$	$w_i$
$t_{po}$	0
$t_{pi}$	0
$t_m$	0
$t_{Si}$	100
$t_{PZT}$	120

## 2.2 FE-Analysis

To evaluate the model in an iterative design process, the commercial finite element software COMSOL Multiphysics 5.6 was used. Both structures are believed to be thin in comparison with the length. Therefore, the structures were assigned with two dimensional triangular shell element. The domain of the structures were assigned with a uniform mesh. A mesh convergence study was carried out to validate the resulting bandwidth and tolerance.

### 2.2.1 Piezoelectric model

In COMSOL, the structures were modelled using the layered shell module. The silicon layer was assigned to be linear elastic while the PZT layer was assigned to be piezoelectric. The proof masses were considered as part of the silicon layer and were treated as linear elastic. A layered material was created to define the material of the combined parts of the structure. The combined parts are the beams, which consist of silicon and PZT. The proof masses were assigned with a material that only consists of silicon. A continuity boundary condition were defined on the edges where the layered material transition to the silicon layer.

Electric insulation enfold the parts assigned with the piezoelectric material. This was done in order to ensure that no electric current may escape from the piezoelectric layer. Ground potential was assigned to the boundary between the silicon and the PZT in the layered shell. The initial geometry in COMSOL can be seen in Figure 2.5, where the single fold is positioned to the left and the double fold to the right.

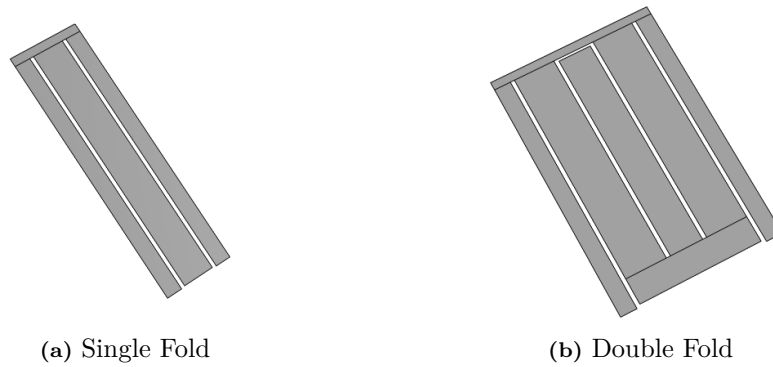


**Figure 2.5:** Initial geometry in COMSOL of the Single fold (a) and the double fold generator (b).

### 2.2.1.1 Boundary Condition

A prescribed displacement  $d$  was defined on the edges of the outer beam seen in Figure 2.1 and 2.3. The prescribed displacement is considered as the amplitude of a harmonic oscillation according to

$$z(t) = d \sin(\omega t) \quad (2.1)$$

where  $\omega$  is the angular frequency  $\omega = 2\pi f$ . As the ambient sources can move the energy generator in any direction, the problem is simplified to only consider out of plane motion. This means that direction  $x$  and  $y$  are prescribed to zero. The constant amplitude  $d$  of the harmonic oscillation was derived by taking the derivative two times on equation (2.1) with respect to time. By doing this, the acceleration was obtained according to

$$\frac{d^2 z(t)}{dt^2} = -d\omega^2 \sin(\omega t) = a(t) = -\bar{a} \sin(\omega t) \quad (2.2)$$

Here, the constant acceleration  $\bar{a}$  was assumed to be  $1g = 9.81 \text{ ms}^{-2}$ . By canceling the sine terms, the equation resulted in the amplitude being dependant on the angular frequency according to

$$d = \frac{9.81}{(2\pi f)^2} \quad (2.3)$$

For simplicity, the frequency  $f$  was assumed to be 2000 Hz for all frequencies. This resulted in a constant amplitude  $d = 0.12 \mu\text{m}$  for all frequencies in the frequency response study [2].

### 2.2.1.2 Damping

Both material models were complemented with mechanical damping. A damping matrix cannot be directly constructed by identifying the material and size. For this work, the Rayleigh damping model was used. The model is a linear combination of the mass and stiffness matrices according to

$$\mathbf{C} = \alpha \mathbf{M} + \beta \mathbf{K} \quad (2.4)$$

The coefficients  $\alpha$  and  $\beta$  are given by equation (2.5)

$$\begin{bmatrix} \alpha \\ \beta \end{bmatrix} = \frac{8\pi^2 f_1 f_2}{4\pi^2 (f_2^2 - f_1^2)} \begin{bmatrix} 2\pi f_2 & -2\pi f_1 \\ -\frac{1}{2\pi f_2} & \frac{1}{2\pi f_1} \end{bmatrix} \begin{bmatrix} \zeta_1 \\ \zeta_2 \end{bmatrix} \quad (2.5)$$

Here  $f_1$  and  $f_2$  are the first and the second eigenfrequencies where the damping is applied. In this work, the problem is simplified by having the damping ratios equal. This means that the coefficients  $\alpha$  and  $\beta$  may be written as [9].

$$\alpha = \frac{4\pi\zeta f_1 f_2}{f_1 + f_2} \quad (2.6)$$

$$\beta = \frac{2\zeta}{2\pi(f_1 + f_2)} \quad (2.7)$$

The damping ratio for both models were assumed to be  $\zeta = 10^{-3}$ . This assumption is based on an experiment done by Shen et al [10]. The experiment was carried out with similar dimensions, material and boundary conditions. Since the double fold generator has presumably three eigenfrequencies, the damping frequencies  $f_1$  and  $f_2$  were applied on the first and second eigenfrequency. This is due to lower order eigenfrequencies are the most dominant and the modes store more energy that requires damping.

## 2.2.2 Simulation Approach

The simulation approach was the same for both models and were split into two subtasks. The initial subtask was to calculate the eigenfrequencies with corresponding mode shape. The second and final subtask was to calculate the frequency response for both models.

### 2.2.2.1 Analysis of Eigenfrequency and Modes Shape

The computation of the eigenfrequencies with the corresponding mode shape was done with the eigenfrequency study in COMSOL. In the study, a parameter sweep was created to iterate through different geometric parameters. The results were investigated whether it brought the eigenfrequencies together or separated them. The mode shapes were also studied in order to understand what parameter may close the gap between the eigenfrequencies. This process was repeated until the eigenfrequencies were reasonably close.

### 2.2.2.2 Analysis of frequency response

The next step was the computation of the frequency response. This was done with the frequency domain study in COMSOL. A frequency range was created which was based on the frequency gap to ensure that the bandwidth was covered. The iteration of design parameters was carried out with respect to the improvement of bandwidth and tolerance.

## 2.2.3 Post processing

Raw data obtained by COMSOL were mainly post processed in Matlab for visualization. The electric potential was extracted from the top layer of the piezoelectric material. The extraction was done by taking the surface average of the selected domain. The electric potential of the outer and inner beam was treated separately. The total electric potential output of the single fold generator was considered to be the sum of the surface average according to equation (2.8). Furthermore, if the double fold generator was considered, the equation would be expanded to include an additional inner beam and a middle beam according to equation (2.9).

$$U_{s,tot} = 2|\bar{U}_{out}| + |\bar{U}_{in}| \quad (2.8)$$

$$U_{d,tot} = 2|\bar{U}_{out}| + 2|\bar{U}_{in}| + |\bar{U}_{mi}| \quad (2.9)$$

Geometry parameters were updated if the total output increased the bandwidth or the tolerance. The bandwidth  $b_f$  is defined by a minimum threshold of  $V_{th} = 0.1$  V. This is considered to be the minimum voltage output that can be harvested by the generator [2]. The tolerance  $\delta$  is defined as the lowest value between the inter valley peaks of the eigenfrequencies on the frequency response curve with respect to the threshold. The tolerance is calculated according to equation (2.10).

$$\delta = \frac{V_{low} - V_{th}}{V_{th}} \times 100 \% \quad (2.10)$$

Here  $V_{low}$  is the lowest electrical potential between the inter peak valley of the frequency response curve. The bandwidth and the voltage difference are illustrated in Figure 2.6 below.

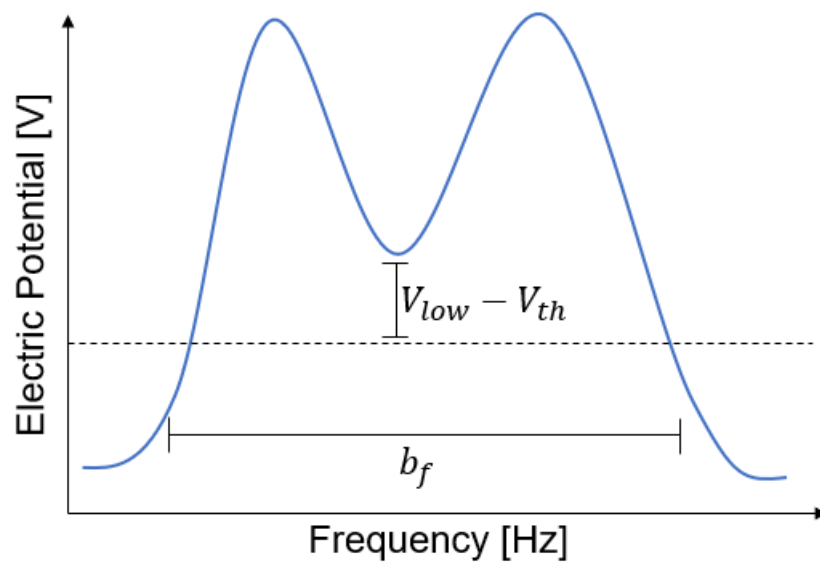


**Figure 2.6:** Illustration of bandwidth and tolerance on the frequency response curve.

# 3

## Results

This section covers the resulting design and the procedure of the single and double fold generator. Each design process is divided into two subsections. The first section presents the results obtained by the eigenfrequency analysis. The second part is the frequency response. Each section describes the design process and the improvement made to optimize the design with respect to the limitations.

### 3.1 Single Fold Generator

#### 3.1.1 Eigenfrequencies and mode shape

The initial geometric dimensions of the single fold generator were based on a thickness layup of 20  $\mu\text{m}$  silicon with a PZT layer of 1  $\mu\text{m}$  [2]. The current design with the updated thickness layup resulted in a much higher frequency range. A frequency study with a parameter sweep over different outer beam lengths were created and the result is viewed in Figure 3.1. The result shows that it is desired to utilize the complete length specified in the limitations to lower the frequency range. Additionally, the gap between the frequencies are also lowered. The length ratio between the inner and outer beams were left unchanged.

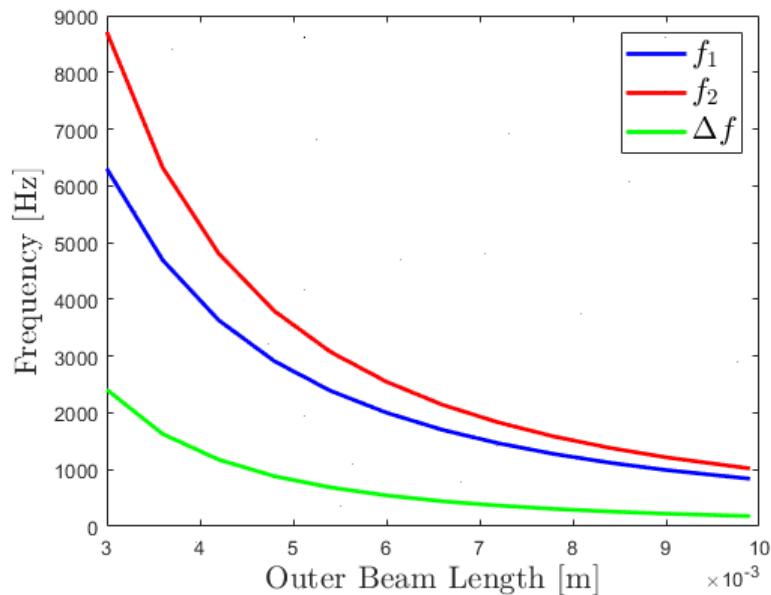


**Figure 3.1:** Frequency study with a parameter sweep over different outer beam lengths.

The additional length of the structure would induce an unwanted mode shape. The second mode shape shows in plane motion seen in Figure 3.2. It is highly desired to have out of plane motion since in plane motion may cause damage to the structure. This was mitigated by increasing the outer beam width, which is shown in Figure 3.3.

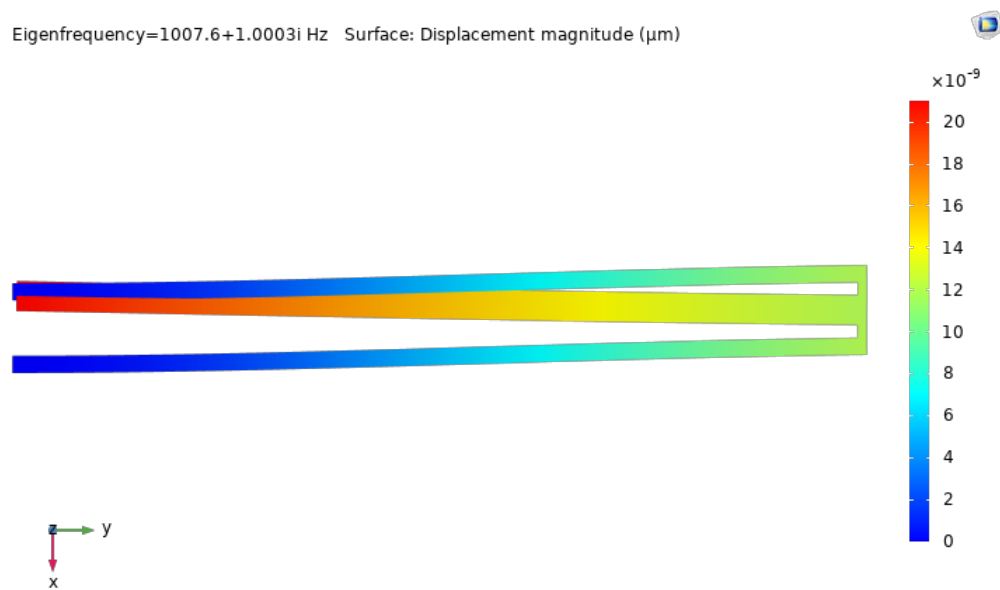


**Figure 3.2:** Second mode shape of the single fold generator showing in plane motion. The deflection is not to scale.

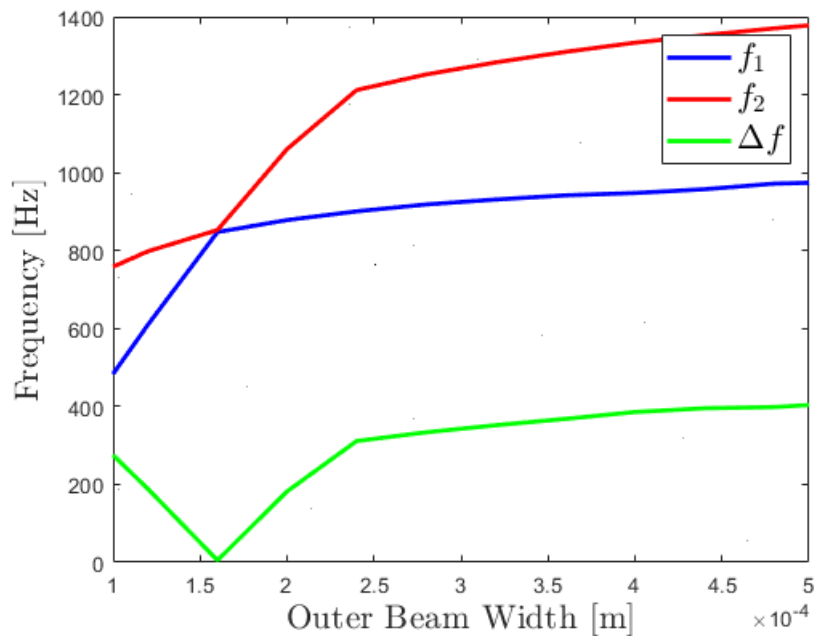


**Figure 3.3:** Frequency study with a parameter sweep over different outer beam widths.

The eigenfrequency parameter sweep in Figure 3.3 shows the effect of varying the width of the outer beam. The unwanted mode shape is removed with width of  $250 \mu\text{m}$ . By doing this, the unwanted mode shape was switched to a higher order and the second mode shape is replaced with a mode shape that moves in the out of plane direction. It was decided to use a width of  $400 \mu\text{m}$  to ensure correct out of plane movement by the second mode shape. The gap between inner and outer beams were increased by a factor of 3 to  $150 \mu\text{m}$ . This change did not worsen the eigenfrequency range nor the gap. Instead, this change was done due to benefiting the fabrication process of the structure. The out of plane movement by the sought first and second mode shapes are shown in Figure 3.4 and 3.5 respectively.

Eigenfrequency= $872.06+0.89816i$  Hz Surface: Displacement magnitude ( $\mu\text{m}$ )

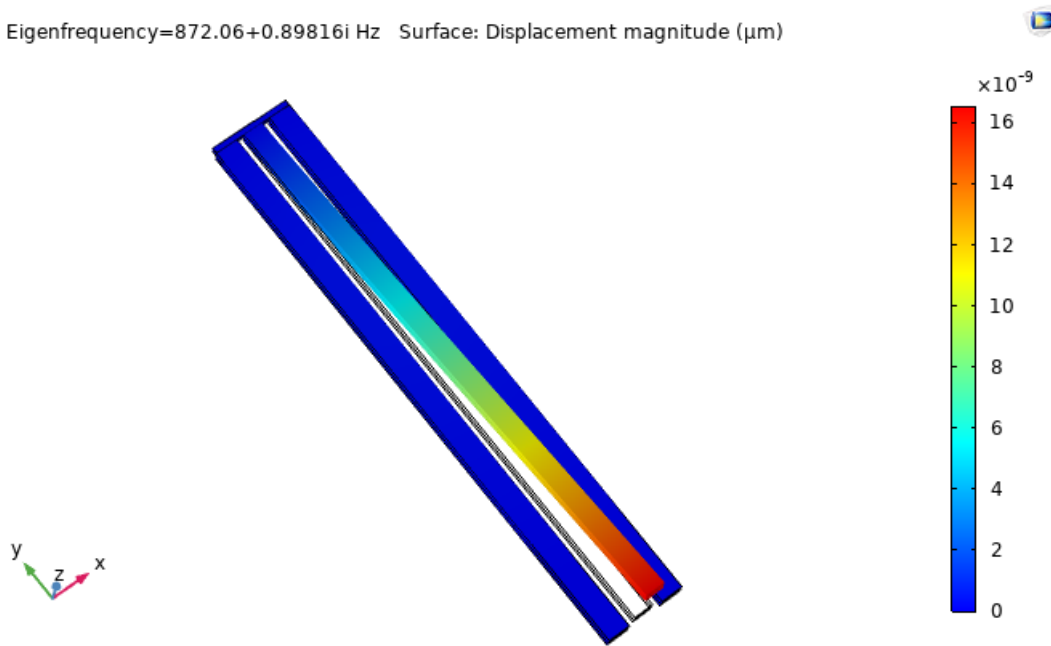


**Figure 3.4:** First mode shape of the single fold generator. The deflection is not to scale.

Eigenfrequency= $1331.9+1.3099i$  Hz Surface: Displacement magnitude ( $\mu\text{m}$ )

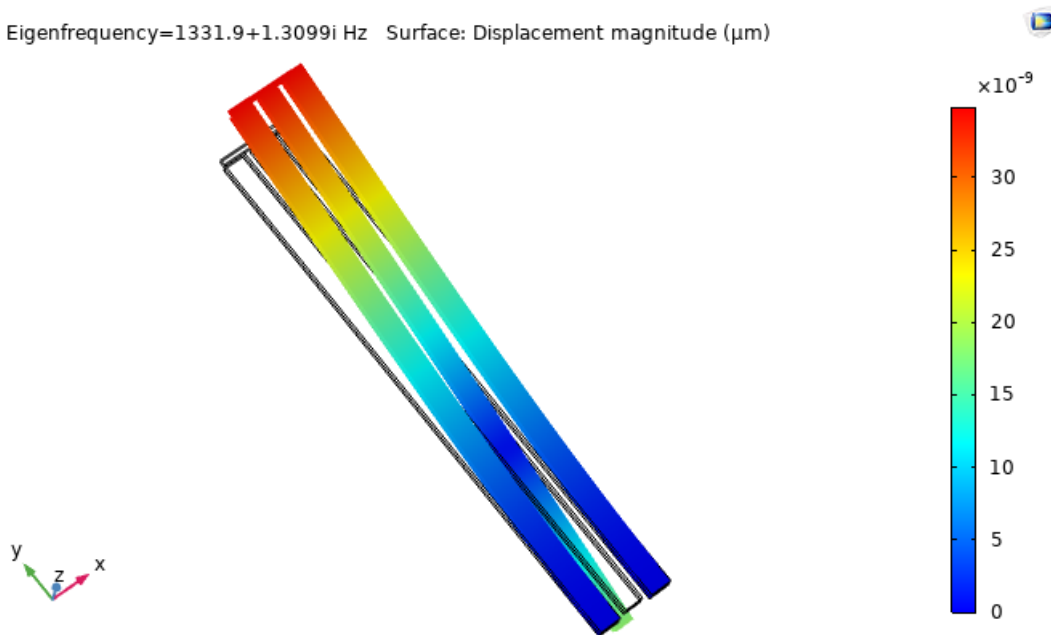


**Figure 3.5:** Second mode shape of the single fold generator. The deflection is not to scale.

### 3.1.2 Frequency Response

Once the frequency range and the gap were brought low and close respectively, the next step was to investigate the frequency response of the structure. It was discovered that the eigenfrequency gap should be around 400 Hz to be considered close enough for bandwidth optimization with respect to frequency response. The first parameter investigated was the length of the outer proof mass  $l_{po}$  from Table 2.1. The frequency response was initially carried out with a frequency range of (1100, 2500) Hz. However, this frequency range was altered depending on where the resonant frequencies occurred to ensure full coverage of the bandwidths. The frequency increment size was 1 Hz for all frequency response studies.

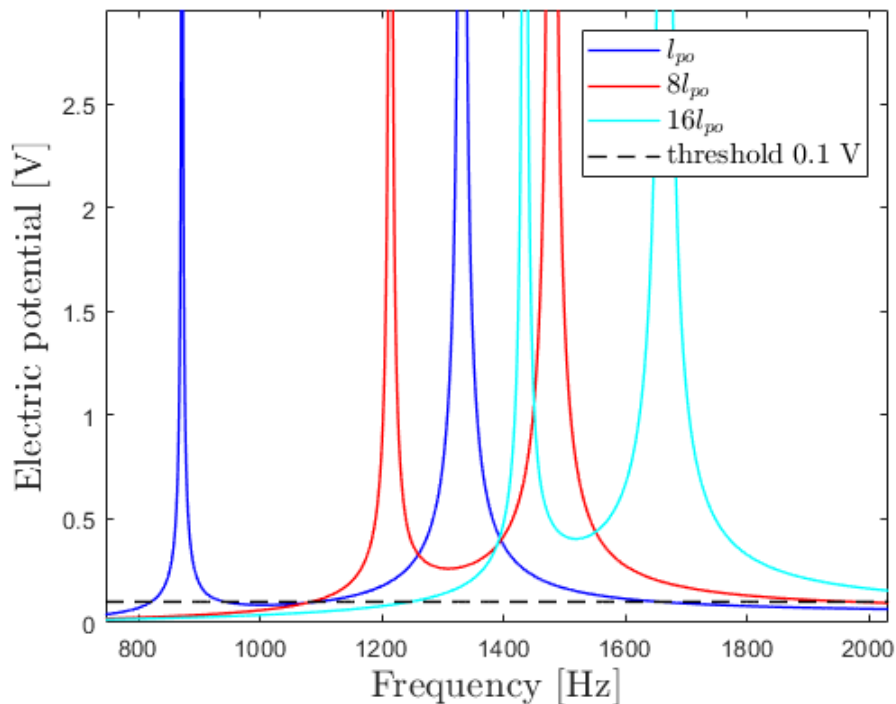


**Figure 3.6:** Frequency response for three different measures of the outer proof mass  $l_{po}$ .

The frequency response shown in Figure 3.6 shows that with a longer outer proof mass, the bandwidth is increased. In addition to the bandwidth, the tolerance of the inter peak valley was increased. However, the increased length of  $l_{po}$  also resulted in a higher frequency range for the operating bandwidth. Since there was no further investigation of the trade of between frequency range and bandwidth, the outer proof mass was decided to be  $l_{po} = 1600 \mu\text{m}$ .

The inner beam was initially free from any proof mass with no mass added in the out of plane direction. However, a study was carried out if a section without any PZT-layer would be beneficial. The resulting frequency response of different inner proof mass lengths are shown in Figure 3.7. In this figure, it is difficult to see any difference in bandwidth. Therefore, an additional plot was created to see the impact of the inner proof mass length with respect to bandwidth. This is viewed in Figure 3.8. This Figure shows that it was favourable with no inner proof mass at all. Instead, the inner beam was chosen to be fully covered with a the PZT-layer.

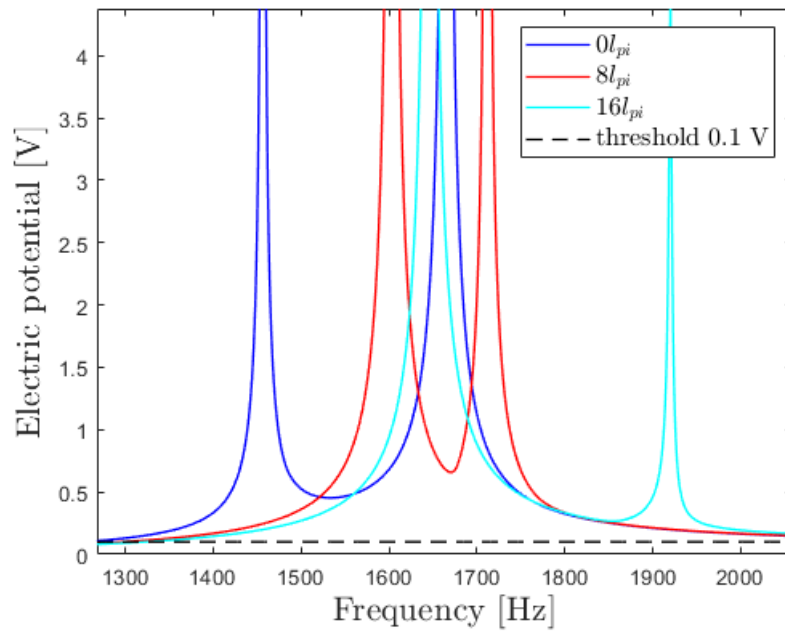


**Figure 3.7:** Frequency response of three different measures of the inner proof mass  $l_{pi}$ .

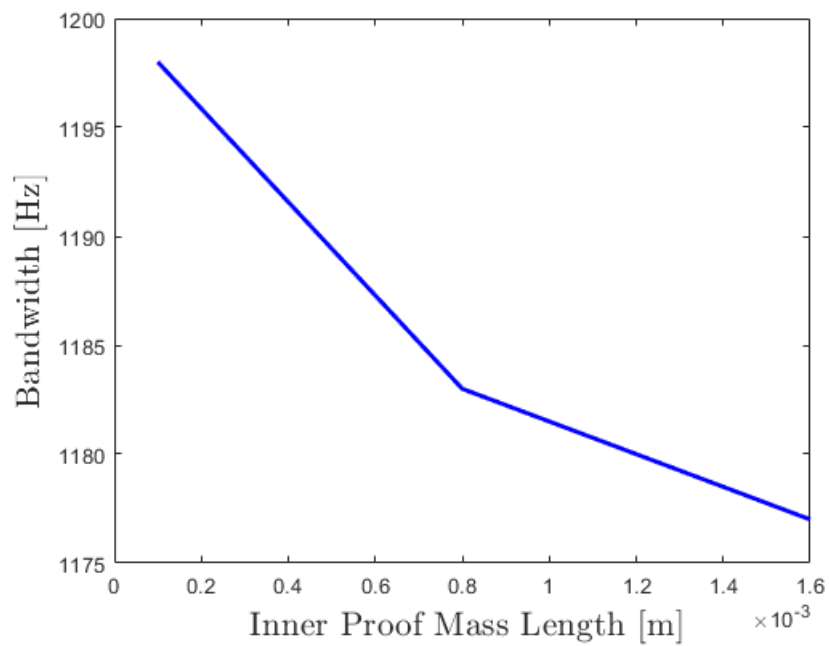


**Figure 3.8:** Bandwidth for three different measures of the inner proof mass length  $l_{pi}$ .

As the single fold generator consists of three different PZT covered beams, each beam generates different levels of electric potential at the resonant frequencies. The inner beam generates a higher electric potential at the first resonant frequency compared to the second. The outer beam generates higher electric potential at the second resonant frequency and is producing a lower level at the first resonant frequency. Overall, the outer beams are generating a higher level of electric potential than the inner beam. This is illustrated in Figure 3.9. With a damping ratio of  $\zeta = 0.001$ , the highest electrical potential for the inner beam is 6.1 V, while the outer beams at the second resonant frequency generates 12.45 V. By adding the electrical structure generated by the beams according to equation (2.8), the total frequency response of the structure may be obtained. The total frequency response with the updated geometry is shown in Figure 3.10.

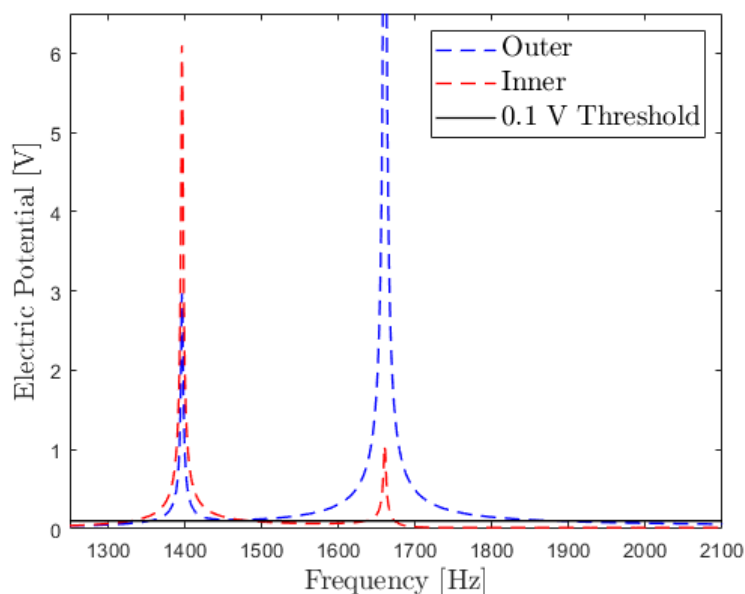


**Figure 3.9:** Frequency response for each PZT covered beam.

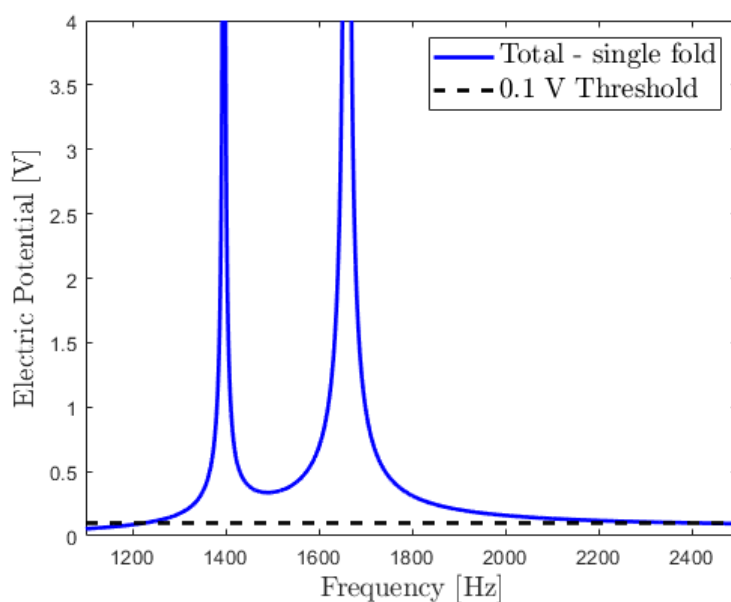


**Figure 3.10:** Frequency response of the total output from the structure.

In order to validate the resulting bandwidth and tolerance, a mesh convergence study was carried out. With the final design parameters in Table 3.1, the operating bandwidth converged to 1181 Hz. The tolerance was calculated according to equation (2.10) and the resulting tolerance became 236%. The convergence of the operating bandwidth and tolerance is illustrated in Figure 3.11. The operating bandwidth appears in the frequency spectrum between 1100 and 2500 Hz. The first resonant frequency appears at a frequency of 1397.2 Hz, while the second resonant frequency appears at 1660.4 Hz.

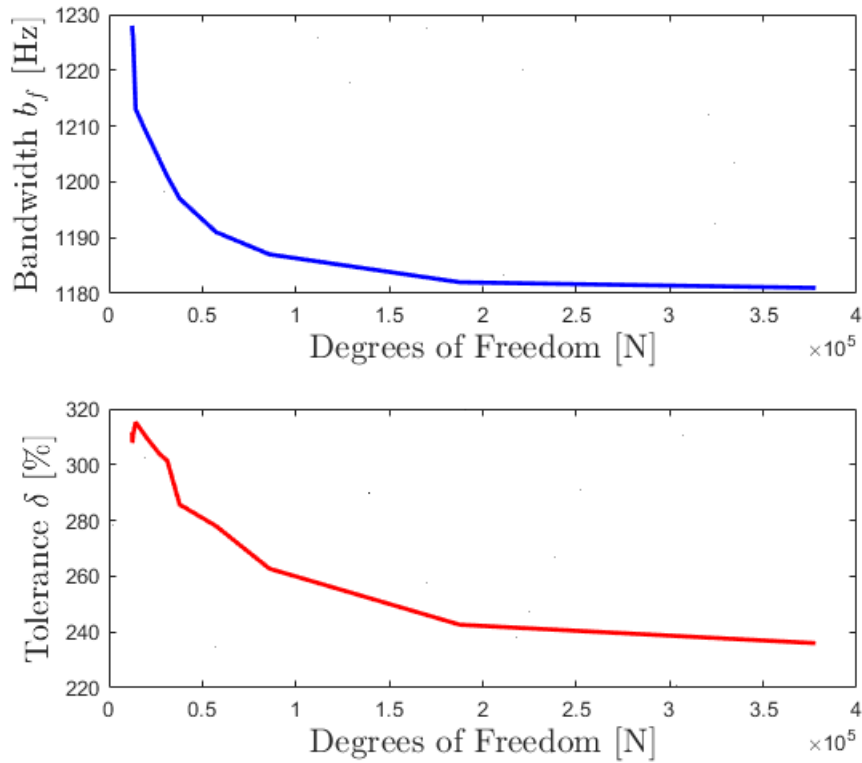


**Figure 3.11:** Mesh convergence plot for with respect to bandwidth  $b_f$  (upper) and tolerance  $\delta$  (lower).

**Table 3.1:** Final design parameters for the single fold generator. All measures are in  $\mu\text{m}$

$l_o$	8400
$l_i$	8358
$l_{po}$	1600
$l_{pi}$	0
$w_o$	400
$w_i$	350
$w_g$	150
$t_{po}$	0
$t_{pi}$	0
$t_{Si}$	100
$t_{PZT}$	120

## 3.2 Double Fold Generator

### 3.2.1 Eigenfrequencies and mode shape

Similarly to the single fold generator, the outer beam length of the double fold generator has a major impact on the resonant frequencies and the gap between them. The frequency study of the outer beam length is shown in Figure 3.12. Likewise the single fold generator, the increased length of the structure induces in plane motion of the second mode shape seen in Figure 3.13. This was mitigated by increasing the outer beam width of the structure similarly to the single fold generator.

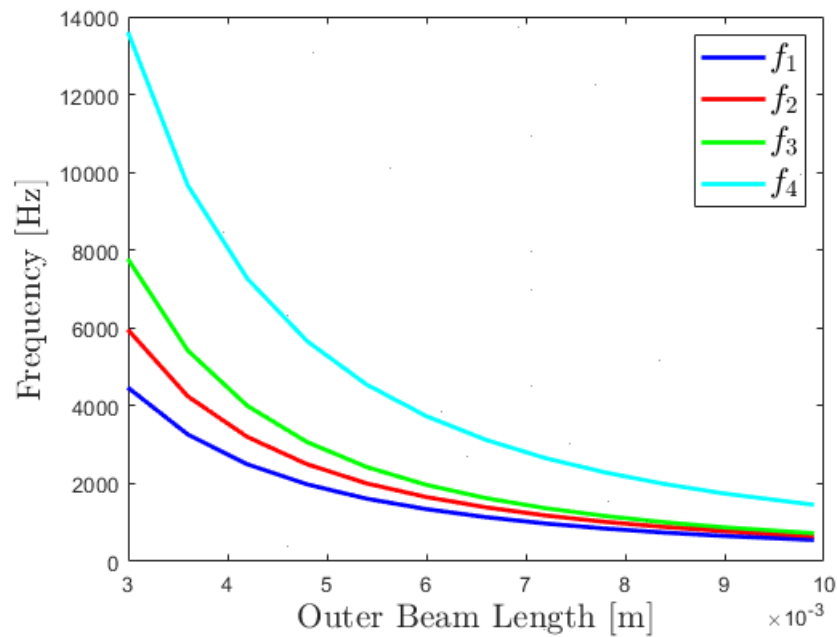


**Figure 3.12:** Frequency study with a parameter sweep over different outer beam lengths

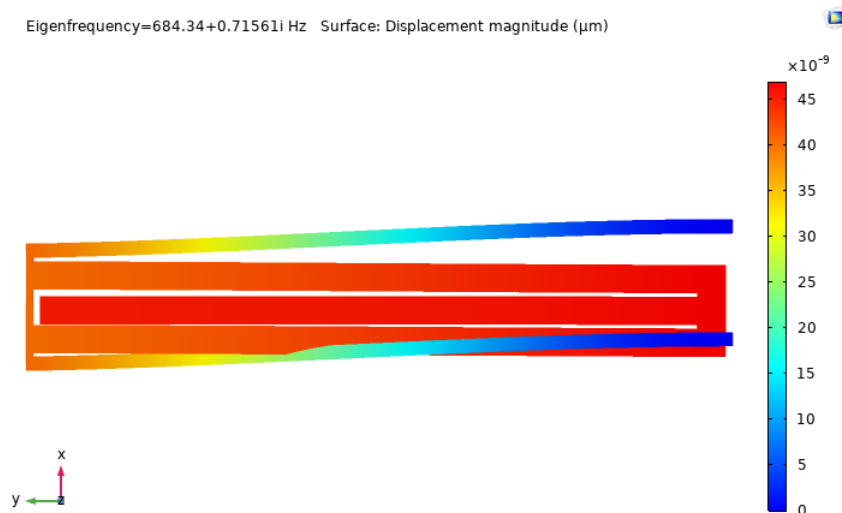


**Figure 3.13:** Second mode shape of the double fold generator showing in plane motion.

For double fold generator, it was beneficial to increase the width of  $w_o = 1500 \mu\text{m}$ . By doing this, the second mode shape is switched to a higher order. The switch is observed with a width of  $w_o \approx 520 \mu\text{m}$ , which is shown in Figure 3.14. Increasing the width even further resulted in a decreased gap between second and third resonant frequency. Additionally, the fourth resonant frequency, which was the new in plane motion, was pushed higher up in the frequency spectrum. The width of the inner beam was increased to  $w_i = 500 \mu\text{m}$ . The reason for this was that the gap between second and third resonant frequency decreased. Changing the gap  $w_{go}$  between the outer beam with the inner beam did not improve the resonant frequency gap. Therefore, the gap was left unchanged. The same case was also observed with the gap between the inner and middle beam.

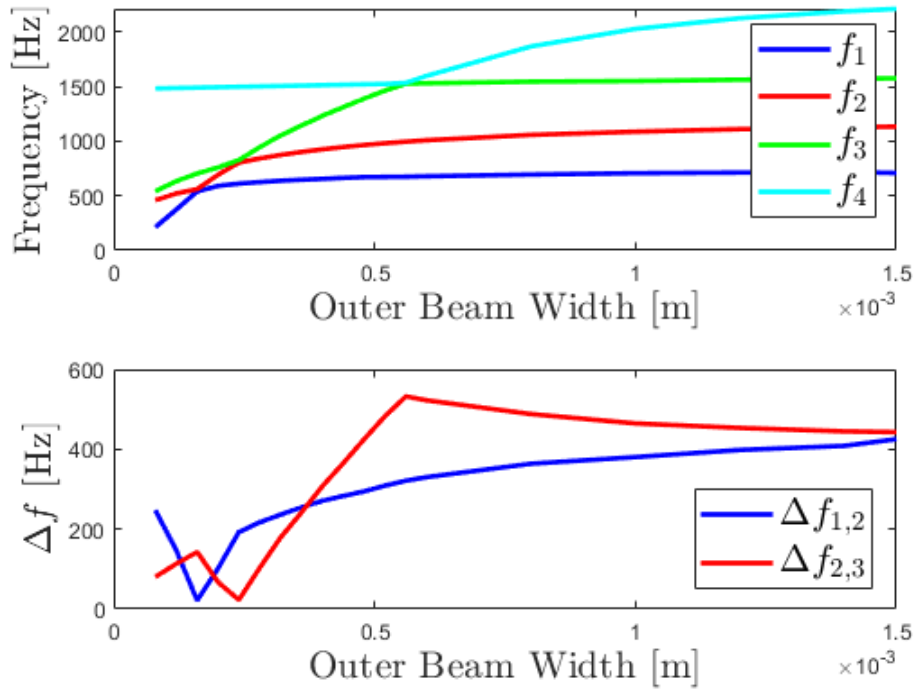


**Figure 3.14:** Frequency study with a parameter sweep over different outer beam widths.

The middle beam width  $w_m$  was decreased to a width of  $320 \mu\text{m}$ . The reason for this was that the second resonant frequency gap were decreased. This frequency study is illustrated in Figure 3.15. The gap increase between the first and second resonant frequency was decreased later by increasing the length of the outer proof mass length seen in Figure 3.17.

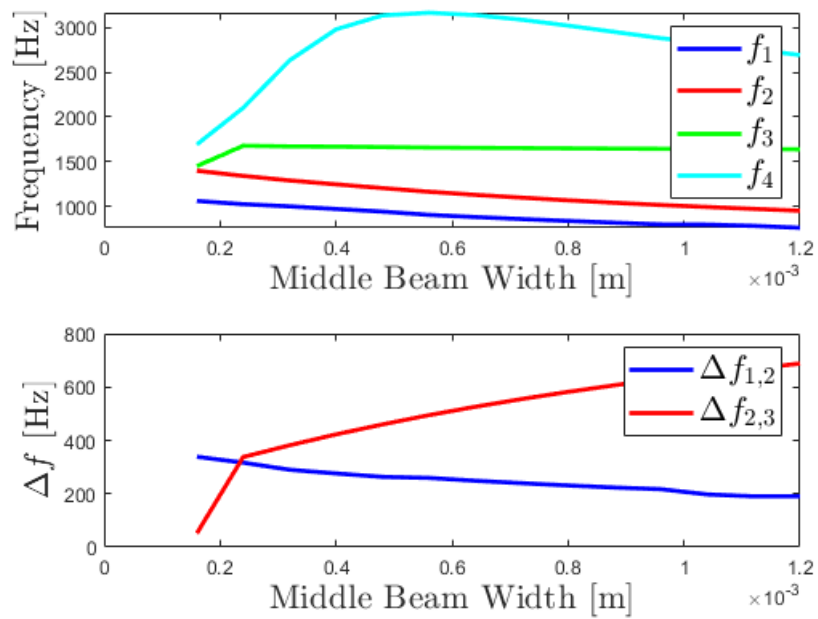


**Figure 3.15:** Frequency study with a parameter sweep over different outer beam widths.

The updated geometry resulted in mode shapes that only moves in the out of plane direction. In the first mode shape, the inner and middle part of the beam are moving in the same direction, while the second mode shape induce movement in the opposite direction. The third mode shape induces movement on the outer and middle part of the structure. Additionally, the movement of the middle and outer parts are in opposite to each other. Each mode shape is presented in the Figure 3.16 below.

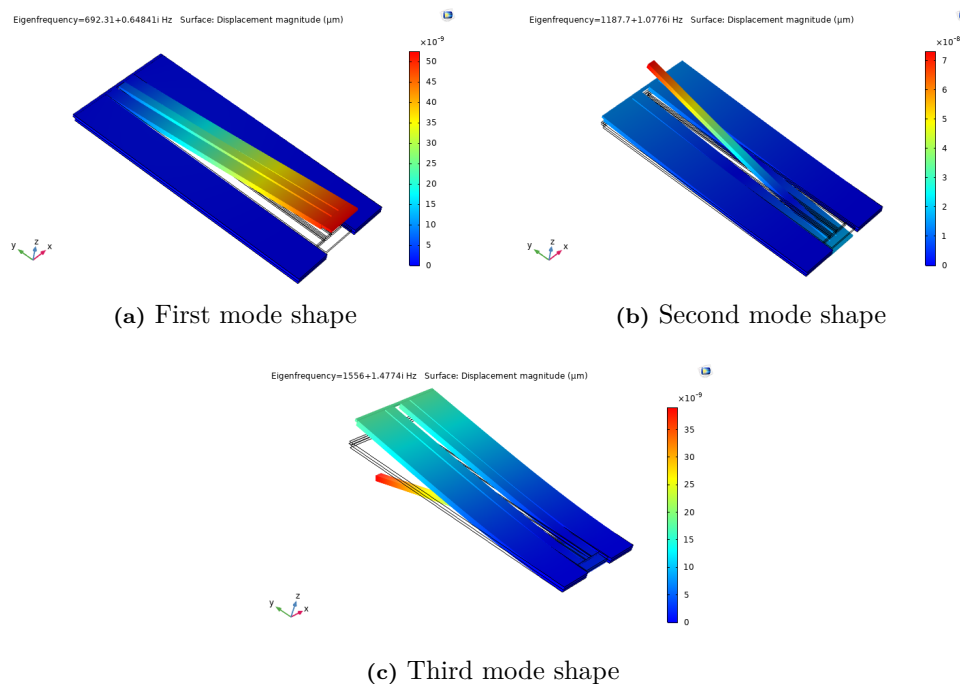


**Figure 3.16:** updated geometry of the double fold generator showing first mode shape (a), second mode shape (b) and the third mode shape(c). The movement is not to scale.

### 3.2.2 Frequency Response

The double fold generator followed the same procedures as the single fold generator. The frequency response was carried out with a frequency range of (400, 2500) Hz. the frequency increment used was 1 Hz for all frequency response studies. First of, the outer proof mass length  $l_{po}$  from Table 2.2 was investigated. Three different measures of  $l_{po}$  were used. The results shown in Figure 3.17 that the tolerance and the operating bandwidth is increased with a longer outer proof mass length. However, the frequency spectrum where the bandwidth is operating is also increased. It was then decided to use a length of 500  $\mu\text{m}$ .

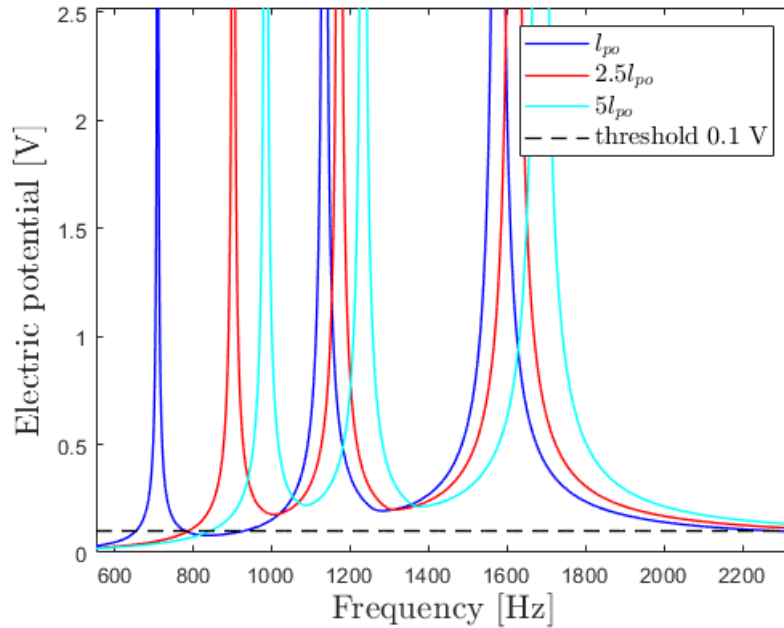


**Figure 3.17:** Frequency response of three different measures of the outer proof mass  $l_{po}$ .

The inner proof mass length  $l_{pi}$ , did not affect the bandwidth the same way as the outer proof mass. This can be seen in Figure 3.18. The result shows that the bandwidth may operate at a lower frequency spectrum if the length is decreased. Since the tolerance for the first and second inter peak valley is decreased, the length was shortened with a factor of 0.8 to  $w_{pi} = 320 \mu\text{m}$ . The length of the proof mass located on the middle beam did not have any significant impact on the bandwidth nor the tolerance. It was then decided to not change the initial design of the middle beam with respect to the proof mass.

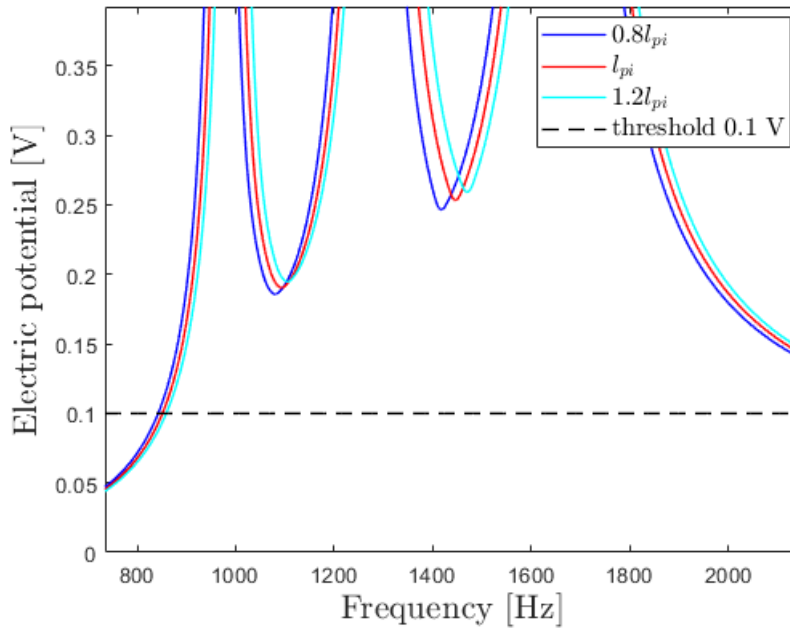


**Figure 3.18:** Frequency response of three different measures of the inner proof mass  $l_{pi}$ .

Similarly to the single fold generator, this structure induces electrical potential on each beam. On the double fold generator, the middle beam contributes with an additional source of electric potential. The frequency response for each beam are illustrated in Figure 3.19. Each beam is then added together according to equation (2.9) and the resulting frequency response with the updated geometry are shown in Figure 3.20. These results show that middle beam is the part that contribute with the most electric potential, while the outer beam gives lower electric potential in comparison with the inner beam. However, since there are two outer and inner beam, they will together induce a higher electric potential compared to the middle beam.

The double fold generator has an operating bandwidth between 900 and 2500 Hz. Simulations done with a wide frequency spectrum of 1 to 12 000 Hz resulted in a frequency response that does not go below the threshold of 0.1 V. This means that the bandwidth will at least be 10 000 Hz. Additionally, there are higher order resonant frequencies that occur around 10 000 Hz which may produce large electrical potential output. However, the fourth order mode shape have an in plane motion and it occurs at a frequency of approximately 2500 Hz.

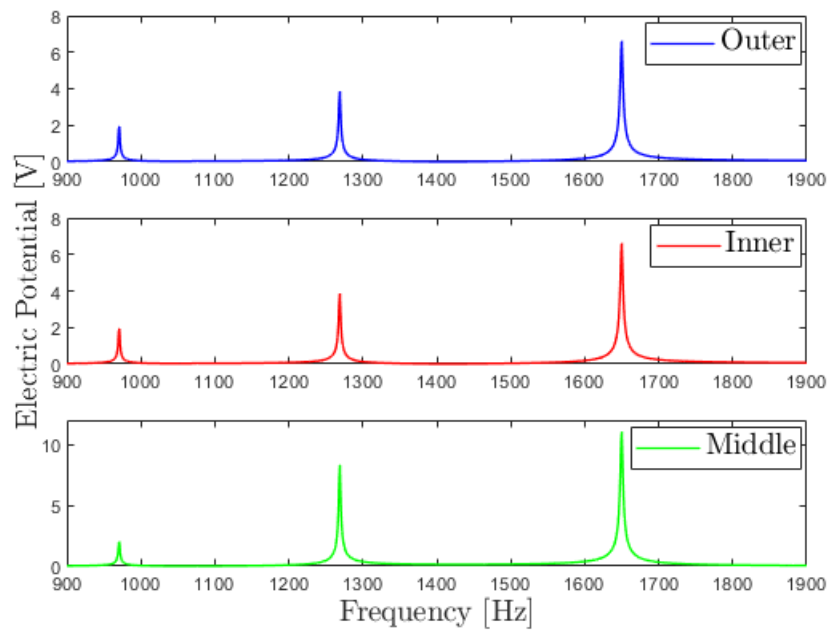


**Figure 3.19:** Frequency response of three different measures of the inner proof mass  $l_{pi}$ .

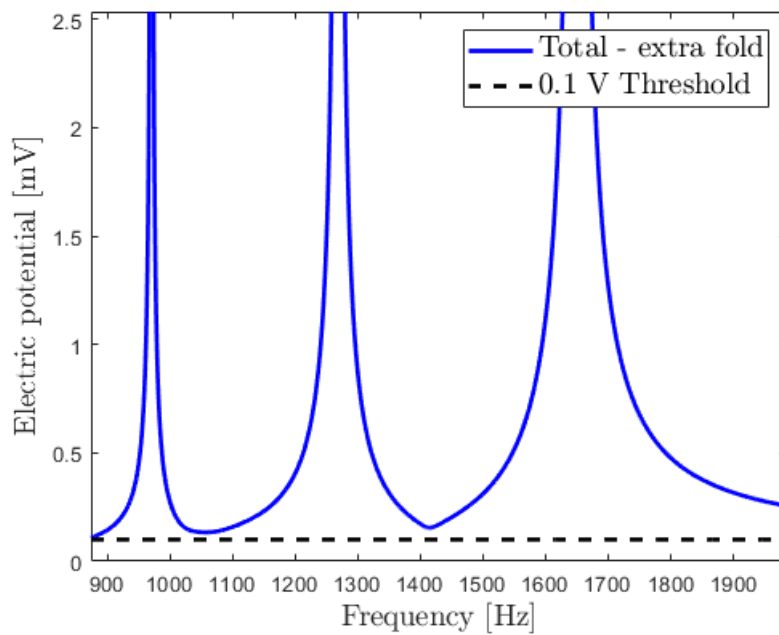


**Figure 3.20:** Frequency response of the total output from the structure

Since it is difficult to define the end of the operating bandwidth of the double fold generator, the mesh convergence study was carried out on the first and second tolerance. The tolerance at the inter peak valley between the first resonant frequency converged to 27.6%. The second tolerance that occur in the valley between the second and third resonant frequency converged to 50.1%. The first, second and third resonant frequency is observed at 954.31 Hz, 1259.8 Hz and 1637.6 Hz respectively. The convergence study was carried out with the final design parameters which is presented in Table 3.2, while the convergence study is viewed in Figure 3.21.

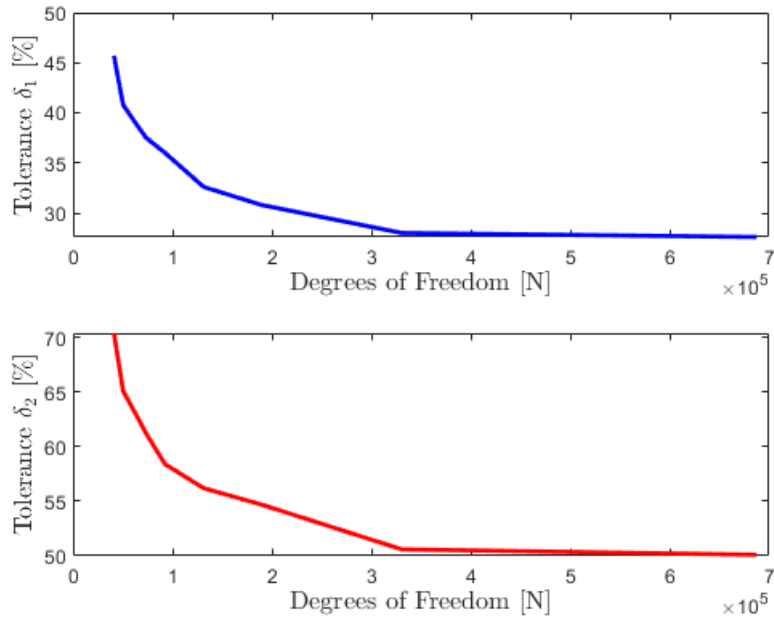


**Figure 3.21:** Mesh convergence plot for with respect to the first tolerance  $\delta_1$  (upper) and second tolerance  $\delta_2$  (lower).

**Table 3.2:** Final design parameters for the double fold generator. All measures are in  $\mu\text{m}$ .

$l_o$	3000
$l_i$	2990
$l_m$	2980
$l_{po}$	100
$l_{pi}$	0
$l_{pm}$	0
$w_o$	200
$w_i$	400
$w_{go}$	50
$w_{gi}$	$w_{go}$
$w_m$	$w_i$
$t_{po}$	0
$t_{pi}$	0
$t_m$	0
$t_{Si}$	100
$t_{PZT}$	120

# 4

## Discussion

The resulting frequency response for the single fold generator shows that it is possible with the geometrical limitations to design a structure that generates electrical potential above the allowable threshold. The length of the structure had the most impact on the frequency range and the resonant frequency gap. Since a resonant frequency gap is not necessarily bad for the bandwidth, the optimisation was carried out with frequency response studies. The outer proof mass length had large impact on the frequency range, tolerance and bandwidth. The range may be explained by having the outer proof mass longer gives a shorter beam structure, which then result in faster vibration. Hence increasing the frequency range of the operating bandwidth. The tolerance and the bandwidth may be explained by having a larger mass at the end may increase the amplitude of the oscillations. This may increase the electric potential output at the resonant frequencies. Thus increasing the voltage level of the bandwidth and tolerance. However, this depends heavily on the damping ratio, which is based on a experiment done on a similar beam design. Simulations were carried out with different damping ratios which resulted in no significant change in bandwidth nor tolerance. The maximum electric potential at resonant frequency was heavily affected by the change of damping ratio.

The double fold generator did show similar behavior with the increased length of the structure. This may be observed by looking at Figure 3.1 and 3.12. However, the structure of the double fold generator proved to be more difficult to optimize with respect to frequency gap. While increasing the outer beam width resulted in an increase of the resonant frequency gap for the first and second gap, the middle and inner beam width increased the first gap and decreased the second gap. Despite producing an intersection point, the results from the frequency response did show that an equal distance between each gap was not beneficial in terms of bandwidth and tolerance. The reason for this may be that difference in electric potential output is difference for each resonant frequency. As the electric potential output is higher at the second and the third resonant frequency, the tolerance is larger at the second valley. This may be seen in the Figure 3.19. This theory is also supported by the convergence study shown in figure 3.21, where it is shown that the second tolerance is larger than the first.

By comparing the two different models, the frequency response of the single fold generator have a better tolerance between the resonant frequencies. On the other hand, the double fold generator has a larger operating bandwidth. Furthermore, the operating bandwidth of the double fold generator starts earlier in the frequency spectrum. This allows for generating electric potential at a lower frequency. In terms of geometry, both models maximize the limitation of the outer length. Also, the double fold generator is almost three times wider than the single fold generator.

The threshold used in the frequency response study has a major affect on the resulting bandwidth and tolerance. If the threshold would increased with a factor of two, then the lowest electric potential in the inter peak valley for the double fold generator would be below the threshold. This would result in a negative tolerance and a small discontinuous bandwidth. On the other hand, the single fold generator would still produce a continuous bandwidth of approximately 500 Hz with a positive tolerance.

Due to slowing down the fabrication process, the cases of varying the thickness of the proof masses were not investigated. It is believed that the structure may be improved even further with in-

creased thickness of the proof masses. The increased thickness may result in larger amplitude at resonant frequencies and also lower the frequency spectrum where the bandwidth is operating. A different approach could be to add another fold to the model to induce more resonant frequencies closer to each other.

# 5

## Conclusion

The results conclude that the final design of the single fold generator resulted in a bandwidth of 1181 Hz operating between 1100 and 2500 Hz with a tolerance of 236 %. The final design of the double fold generator resulted in a bandwidth of at least 2500 Hz operating between 900 and 2500 Hz with a tolerance of 27.6 % and 50.1 %. The bandwidth for both models were calculated with respect to a 0.1 V threshold. The key factors observed in the design process were beam length, outer proof mass length and width of the beams.

Both models operates in the same frequency region. However, the single fold generator is superior in terms of tolerance in the inter peak valleys. On the other hand, the bandwidth of the double fold generator is larger than the single fold generator with respect to the minimum threshold of 0.1 V.

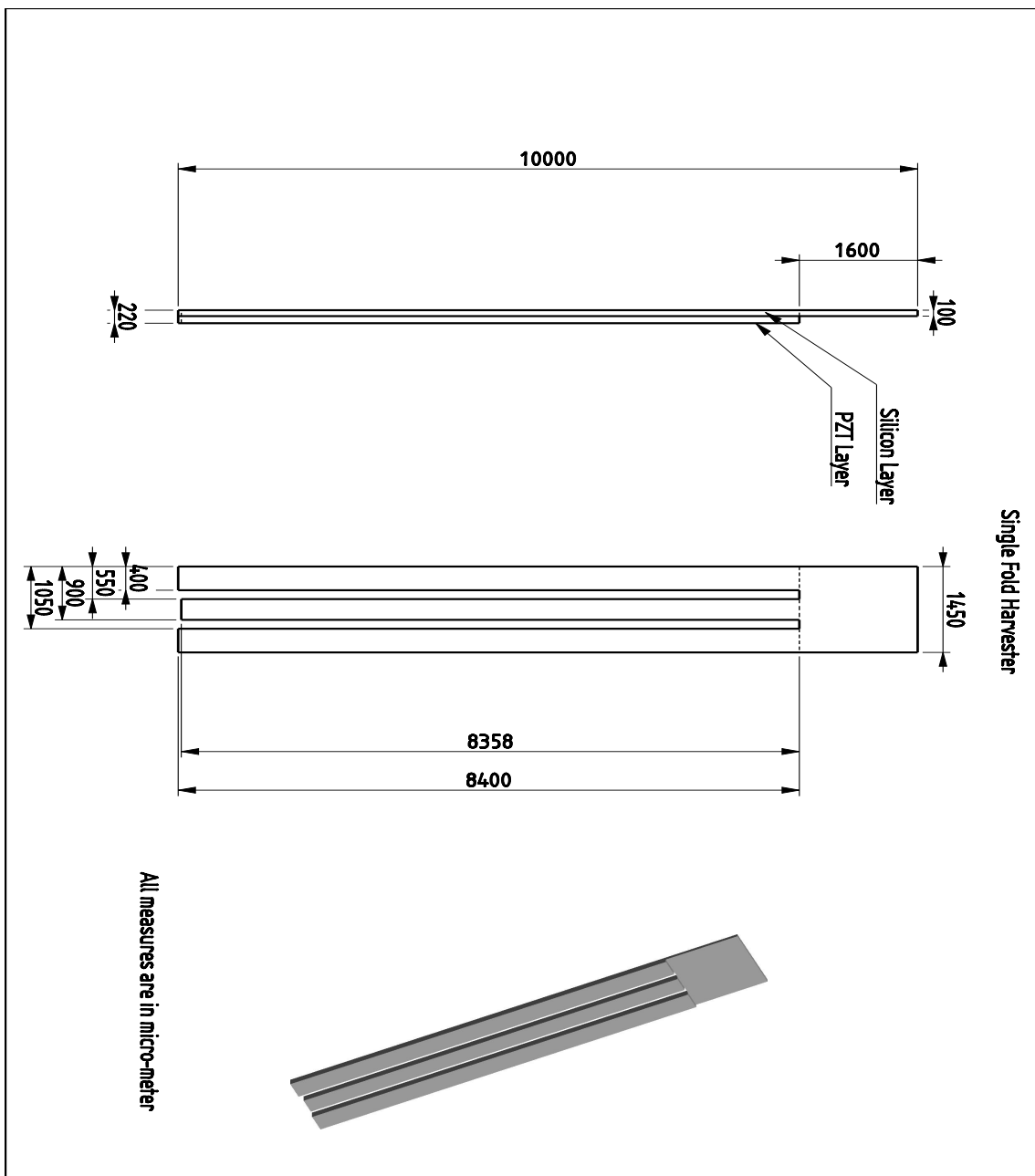
# Bibliography

- [1] Meng Wu, Yi Ou, Haiyang Mao, Zhigang Li, Ruiwen Liu, Ming Anjie, and Ou Wen. Multi-Resonant Wideband Energy Harvester Based on a Folded Asymmetric M-Shaped Cantilever. *AIP Advances*, 5:077149, 07 2015.
- [2] J. Andersson. Bandwidth Improvement of a Piezoelectric Micro Energy Harvester. 2020.
- [3] Gang Tang, Jing quan Liu, Bin Yang, Jiang bo Luo, He sheng Liu, Yi gui Li, Chun sheng Yang, Dan nong He, Viet Dzung Dao, Katsuhiko Tanaka, and Susumu Sugiyama. Fabrication and Analysis of High-Performance Piezoelectric MEMS Generators. *Journal of Micromechanics and Microengineering*, 22(6):065017, may 2012.
- [4] M. Kimura, A. Ando, and Y. Sakabe. 2 - Lead Zirconate Titanate-based Piezo-ceramics. In Kenji Uchino, editor, *Advanced Piezoelectric Materials*, Woodhead Publishing Series in Electronic and Optical Materials, pages 89–110. Woodhead Publishing, 2010.
- [5] Li Jiao Gong, Qiao Sheng Pan, Wei Li, Gang Yi Yan, Yong Bin Liu, and Zhi Hua Feng. Harvesting vibration Energy using Two Modal Vibrations of a Folded Piezoelectric Device. *Applied Physics Letters*, 107(3):033904, 2015.
- [6] H. Staaf. *Conjoined piezoelectric harvesters and Carbon Supercapacitors for Powering Intelligent Wireless Sensors*. PhD thesis.
- [7] Siyang Hu, Sofiane Bouhedma, Arwed Schütz, Simon Stindt, Dennis Hohlfeld, and Tamara Bechtold. Design Optimization of Multi-Resonant Piezoelectric Energy Harvesters. *Microelectronics Reliability*, 120:114114, 2021.
- [8] Agin Vyas, Henrik Staaf, Cristina Rusu, Thorbjörn Ebefors, Jessica Liljeholm, Anderson D. Smith, Per Lundgren, and Peter Enoksson. A Micromachined Coupled-Cantilever for Piezoelectric Energy Harvesters. *Micromachines*, 9(5), 2018.
- [9] Z. Song and C. Su. Computation of Rayleigh Damping Coefficients for the Seismic Analysis of a Hydro-Powerhouse. *Shock and Vibration*, 2017.
- [10] Dongna Shen, Jung-Hyun Park, Jyoti Ajitsaria, Song Choe, Howard III, and Dong-Joo Kim. Design, Fabrication and Evaluation of a MEMS PZT Cantilever With an Integrated Si Proof Mass for Vibration Energy Harvesting. *Journal of Micromechanics and Microengineering*, 18:055017, 04 2008.

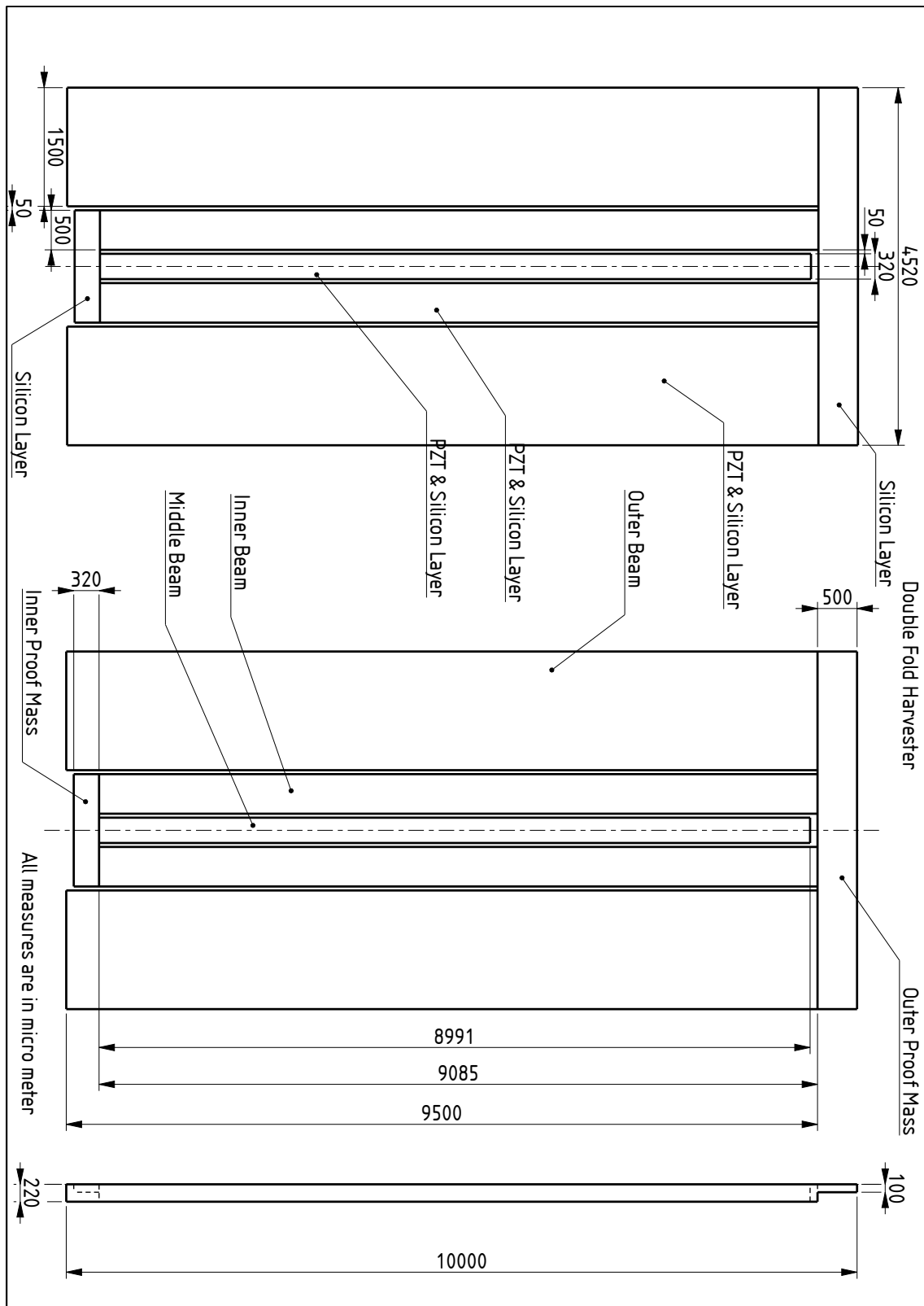
# A

## Appendix

### A.1 Final Design, Single Fold Generator



## A.2 Final Design, Double Fold Generator



DEPARTMENT OF SOME SUBJECT OR TECHNOLOGY  
CHALMERS UNIVERSITY OF TECHNOLOGY  
Gothenburg, Sweden  
[www.chalmers.se](http://www.chalmers.se)



**CHALMERS**  
UNIVERSITY OF TECHNOLOGY